Editors' Suggestion

Fermi-Arc-Induced Vortex Structure in Weyl Beam Shifts

Udvas Chattopadhyay,[1] Li-kun Shi,[2] Baile Zhang,[1,3] Justin C. W. Song,[1,2] and Y. D. Chong[1,3]
[1]Division of Physics and Applied Physics, School of Physical and Mathematical Sciences, Nanyang Technological University, Singapore 637371, Singapore
[2]Institute of High Performance Computing, A*STAR, Singapore 138632, Singapore
[3]Centre for Disruptive Photonic Technologies, Nanyang Technological University, Singapore 637371, Singapore

(Received 17 September 2018; published 13 February 2019)

In periodic media, despite the close relationship between geometrical effects in the bulk and topological surface states, the two are typically probed separately. We show that when beams in a Weyl medium reflect off an interface with a gapped medium, the trajectory is influenced by both bulk geometrical effects and the Fermi arc surface states. The reflected beam experiences a displacement, analogous to the Goos-Hänchen or Imbert-Fedorov shifts, that forms a half-vortex in the two-dimensional surface momentum space. The half-vortex is centered where the Fermi arc of the reflecting surface touches the Weyl cone, with the magnitude of the shift scaling as an inverse square root away from the touching point, and diverging at the touching point. This striking feature provides a way to use bulk transport to probe the topological characteristics of a Weyl medium.

DOI: 10.1103/PhysRevLett.122.066602

Introduction.—One of the most interesting features of wave dynamics in both classical and quantum media is that wave packet trajectories are not determined solely by the dispersion relation, but can also be influenced by the internal structure of the underlying wave functions. For instance, the equations of motion of a wave packet in a periodic medium can include an "anomalous velocity" term tied to the Berry connection of the Bloch functions [1–6]. Another example, originating from the field of optics, involves the displacement of a light beam reflecting off a surface [7]. A lateral displacement is called a Goos-Hänchen (GH) shift [8], while a transverse one is called an Imbert-Fedorov (IF) shift [9], and both originate from the polarization degree of freedom of electromagnetic waves [10,11]. In electronic systems such as strained graphene, similar shifts can be induced by pseudospin degrees of freedom, and are predicted to have observable effects on transport in heterojunction devices [12,13].

Another phenomenon intimately linked to the internal structure of wave functions is the existence of topological surface states, which arise from subtle windings of the Bloch functions in momentum space [14]. For example, three-dimensional Weyl media feature linear band-crossing points called Weyl points that act as monopole sources of Berry curvature in momentum space [15], and cause several nontrivial bulk dynamical effects [16–25]. The net Berry flux between pairs of Weyl points guarantees the existence of "Fermi arcs" of surface states along any interface with a gapped medium [15]. Weyl media have been realized in multiple venues including photonic crystals and waveguide arrays [26–28], materials such as TaAs [29–32], as well as acoustic, mechanical, and electric metamaterials [33–38].

Despite this bulk-edge correspondence, the nontrivial bulk dynamics of Weyl media (a band geometric property) and Fermi arc surface states (a topological property) have largely been probed separately. The former has been studied using spectroscopic tools like angle-resolved photoemission [30], whereas the latter has been studied through bulk transport effects such as negative magnetoresistance [17,22,23] and anomalous Hall conductivity [18]. Another interesting bulk phenomenon in Weyl media involves the GH and IF shifts experienced by a wave packet undergoing partial reflection off a potential step in the bulk [20,21,24,25]. These shifts have been attributed to the Weyl medium's spinor degree of freedom, and the direction of the IF shift has been shown to be determined by the sign of the Weyl point's Berry flux. However, no direct connection to the Fermi arc surface states was identified.

In this Letter, we show that when a beam in a Weyl medium reflects off an interface with a gapped medium, the displacement of the reflected beam exhibits an anomalous half-vortex structure in momentum space. This effect provides a bulk probe of the topological Fermi arc at the reflecting surface. Previous studies into GH and IF shifts in Weyl media dealt with *partial* reflection off a potential step separating two Weyl media [20,21,25]. In contrast, we consider *total* reflection off an interface with a medium that is gapped (i.e., supporting no propagating waves at the operating energy). Unlike a potential step, such an interface features a Fermi arc extending outward from the Weyl cone in the two-dimensional surface momentum space [15]. The real-space displacement of the reflected beam, $\vec{\Delta}$, varies with the direction of the incident beam, which is characterized by its average in-plane momentum $\vec{K}_\perp$. We show

that $\vec{\Delta}(\vec{K}_\perp)$ circulates around $\vec{K}_{\rm fa}$, the point on the boundary of the Weyl cone touched by the Fermi arc, and its magnitude scales as an inverse square root, $|\vec{\Delta}| \sim |\vec{K}_\perp - \vec{K}_{\rm fa}|^{-1/2}$. This behavior is observed in two different Hamiltonian models with distinct boundary condition implementations, indicating that it is generic. In microwave photonic crystals [26], the magnitude of the predicted shift is several multiples of the lattice constant under realistic conditions. The displacement accumulates over successive reflections off two parallel surfaces, and thus affects the effective velocity of propagation [12] in films of Weyl medium. To our knowledge, this is the first prediction of the Fermi arc having observable effects on beam trajectories in Weyl media, which may inspire further studies of the physical effects of Fermi arcs.

Plane waves in a Weyl medium.—We consider the setup shown in Fig. 1(a), where a Weyl medium occupies the space $z > 0$ with a gapped medium in $z < 0$. A monochromatic beam of energy E is incident from the Weyl medium, and reflects off the $z = 0$ surface. The reflected beam can experience a displacement, denoted by a vector $\vec{\Delta}$ parallel to the x-y plane. The reflection is total, for E lies in the gap of the $z < 0$ medium.

The eigenmodes of the bulk Weyl medium are described by a 2×2 Hamiltonian $H_w = \sum_j v_j k_j \sigma_j$, where for each direction $j \in \{1, 2, 3\}$, v_j is the phase velocity, k_j is the wave number, and σ_j is a Pauli matrix. (In quantum mechanical contexts, we set $\hbar = 1$.) The Weyl point possesses a chirality invariant $C = \mathrm{sgn}(v_x v_y v_z)$, which can only be altered by annihilation with another Weyl point [15]. We henceforth take $v_x = v_y = v_z = v$, so that $C = \mathrm{sgn}(v)$. For given $\vec{k}$, the modal eigenenergy (or eigenfrequency) is $E = v|\vec{k}|$, and the wave function is a superposition of two basis wave functions with coefficients given by the spinor components of the envelope function $\psi(\vec{k}, \vec{r}) = \Psi(\vec{k}) \exp(i\vec{k} \cdot \vec{r})$, where $\Psi(\vec{k})$ is an eigenvector of $H_w(\vec{k})$ and $\vec{r} \equiv (x, y, z)$.

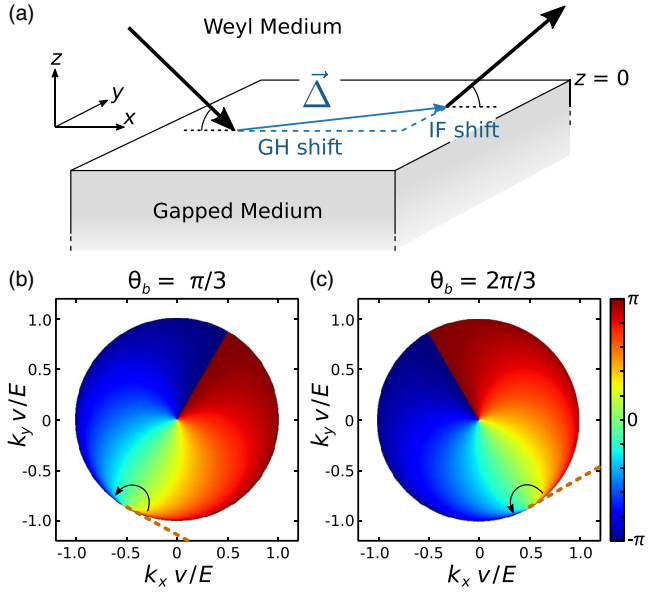

FIG. 1. (a) Schematic of the reflection setup. A beam is incident from a Weyl medium in the space $z > 0$, and reflects off a gapped medium at $z < 0$. The vector $\vec{\Delta}$ denotes the total displacement of the reflected beam. (b)–(c) Map of the reflection phase ϕ experienced by an incident plane wave, versus the in-plane wave numbers k_x and k_y (normalized to E/v). Results are shown for two different values of θ_b, which governs the boundary condition. The Fermi arc is denoted by dashes, and ϕ exhibits a -2π phase shift during a half-encirclement of the Fermi arc's touching point (black arrow).

For incident and reflected plane waves (not beams), the eigenvectors are taken to be

$$\Psi_i = \frac{1}{\sqrt{1+\eta_-^2}} \begin{bmatrix} 1 \\ \eta_- e^{i\alpha} \end{bmatrix}, \qquad \Psi_r = \frac{e^{i\phi}}{\sqrt{1+\eta_+^2}} \begin{bmatrix} 1 \\ \eta_+ e^{i\alpha} \end{bmatrix}, \tag{1}$$

where

$$\alpha = \tan^{-1}\left(\frac{k_y}{k_x}\right), \qquad \eta_\pm = \sqrt{\frac{E - v k_z^\pm}{E + v k_z^\pm}},$$
$$k_z^\pm = \pm\sqrt{(E/v)^2 - |\vec{k}_\perp|^2}. \tag{2}$$

The $k_z < 0$ ($k_z > 0$) branch is chosen for the incident (reflected) wave, and $\vec{k}_\perp$ is the projection of $\vec{k}$ onto the k_x-k_y plane. The $\exp(i\phi)$ factor is a reflection coefficient, determined by the boundary condition at $z = 0$.

From the Hermiticity of the real-space Hamiltonian, one can show [39–41] that the boundary of a Weyl medium is characterizable by a single real angular parameter $\theta_b \in [0, 2\pi]$, such that

$$[1 \; e^{-i\theta_b(\vec{k}_\perp)}]\psi_{\rm tot}|_{z=0} = 0, \tag{3}$$

where $\psi_{\rm tot}$ is the sum of the incident and reflected envelope functions. Note that θ_b may vary with $\vec{k}_\perp$. Hence,

$$e^{i\phi} = -\sqrt{\frac{1+\eta_+^2}{1+\eta_-^2}} \frac{1 + \eta_- e^{i\alpha} e^{-i\theta_b}}{1 + \eta_+ e^{i\alpha} e^{-i\theta_b}}. \tag{4}$$

Equation (3) also yields surface states, which have the form $\psi_s \propto e^{-\kappa z}[e^{-i\theta_b}, -1]^T$ for $z > 0$, where $\kappa = k_x \sin\theta_b - k_y \cos\theta_b \geq 0$. These lie along a Fermi arc [15] given by

$$E = -k_x \cos\theta_b - k_y \sin\theta_b. \tag{5}$$

In this model, the Fermi arc extends to infinity, since there is only a single Weyl cone.

The resulting reflection phase is shown in Figs. 1(b)–1(c), for two representative cases where θ_b is a constant

independent of $\vec{k}_\perp$. The color map gives the values of ϕ within the circular domain $|\vec{k}_\perp| \leq E/v \equiv K_W$, which is a section of the Weyl cone. The Fermi arc lies outside the cone and touches its boundary tangentially. The touching point, and the orientation of the Fermi arc, depend on the choice of θ_b. We see that ϕ winds by 2π during a half-encirclement around the Fermi arc touching point.

These features can be understood by considering the Weyl cone section's boundary, $|\vec{k}_\perp| = K_W$, which is parametrized by the polar angle α [Eq. (2)]. As we approach the boundary from the inside (i.e., real $k_z \to 0$), the expressions for Ψ_i and Ψ_r in Eq. (1) become linearly dependent, so that $\psi_{\text{tot}} \propto (1 + e^{i\phi})\Psi_i$ and $\eta_\pm \to 1$. Hence, the boundary condition (3) can be satisfied in two ways: (i) $\phi = \pi$, so that ψ_{tot} vanishes, or (ii) $\alpha - \theta_b(\vec{k}_\perp) = \pi (\text{mod } 2\pi)$, so that the vectors in Eq. (3) are orthogonal. Case (ii) corresponds to the touching point of the Fermi arc, and when it is satisfied ϕ is undefined rather than being equal to π as in case (i). Evidently, this occurs at a minimum of $|m-1|$ distinct values of α, where m is the winding number of the $\theta_b(\vec{k}_\perp)$ function. We deduce that $m = 0$, which includes the case where θ_b is a constant, describes the class of boundaries between a Weyl medium and a trivial gapped medium. Then there is a minimum of one touching point, and by considering the points just inside the boundary we find that ϕ winds by 2π during a half-encirclement of the touching point [42].

Beams in Weyl media.—A monochromatic beam of energy E can be described as a superposition of planar eigenmodes, with wave numbers $\vec{k}$ constrained by $E = v|\vec{k}|$. The envelope function has the form

$$\Psi(\vec{r}, \vec{K}_\perp) = \int d^2k_\perp g(k_x - K_x) g(k_y - K_y) \psi(\vec{k}, \vec{r}), \tag{6}$$

where $\vec{k}_\perp \equiv (k_x, k_y)$ denotes the in-plane wave vector of each eigenmode, $\vec{K}_\perp$ is the central value for the beam's in-plane wave vector, $g(k_j - K_j)$ is a k-space envelope function, and $\psi(\vec{k}, \vec{r})$ describes a planar eigenmode. We let each g be a Gaussian function of unit area, zero mean, and standard deviation σ_k. For each E, the choice of sign for k_z is determined by the beam direction.

We plug the incident and reflected eigenmodes [Eq. (1)] into Eq. (6), and expand ϕ and α to lowest order, so as to compare the centers of the incident and reflected beams in the $z = 0$ plane. This results in the following formula for the displacement of the reflected beam:

$$\vec{\Delta}(\vec{K}_\perp) = \left(-\nabla_{k_\perp}\phi + \frac{\eta_-^2 - 1}{\eta_-^2 + 1} \nabla_{k_\perp}\alpha \right)_{\vec{k}_\perp = \vec{K}_\perp}. \tag{7}$$

Here, $\nabla_{k_\perp}$ denotes the in-plane k-space derivative, and $\vec{K}_\perp$ is the mean wave vector for the incident beam. Although ϕ, $\eta_\pm$, and α are based on an eigenmode gauge choice [Eq. (1)], the shift (7) is gauge independent. For details, see the Supplemental Material [42].

Figure 2 shows streamline and quiver plots of $\vec{\Delta}$ as a function of $\vec{K}_\perp$. We find that the direction of $\vec{\Delta}$ winds by π during a half-encirclement of the Fermi arc touching-point $\vec{K}_{\text{fa}}$, and moreover that its magnitude scales as

$$|\vec{\Delta}| \sim |\vec{K}_\perp - \vec{K}_{\text{fa}}|^{-1/2}. \tag{8}$$

By analogy with the concept of free vortices from fluid mechanics, we say that $\vec{\Delta}$ exhibits a "half-vortex" structure centered at $\vec{K}_{\text{fa}}$. Note that the shift direction is not purely lateral (GH-like) or transverse (IF-like), but depends on the orientation of the incident beam relative to the Fermi arc. We interpret the formal divergence of $|\vec{\Delta}|$ at $\vec{K}_{\text{fa}}$ to mean that the presence of the Fermi arc causes the beam to deviate significantly from an ideal raylike trajectory. The scaling (8) is observed numerically for different directions stretching away from $\vec{K}_{\text{fa}}$, and we can show that it comes from the $-\nabla_{k_\perp}\phi$ term in Eq. (7); details are given in the Supplemental Material [42]. The analysis also shows that the ϕ vortex at the k-space origin [Figs. 1(b)–1(c)], a feature noted by several previous authors [43–45], does *not* yield a

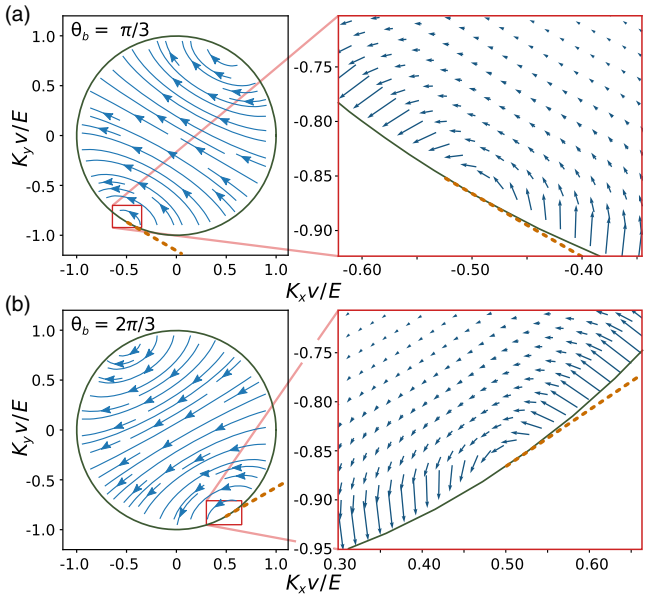

FIG. 2. Maps of the beam shift $\vec{\Delta}$ versus the mean in-plane wave numbers K_x and K_y (normalized to E/v) for the incident beam. Results are shown for two values of the boundary parameter: (a) $\theta_b = \pi/3$ and (b) $\theta_b = 2\pi/3$. In each case, the left panel shows a streamline plot indicating the direction of $\vec{\Delta}$ but not its magnitude; the right panel shows a quiver plot indicating both the direction and magnitude of $\vec{\Delta}$, over a region of K-space surrounding the Fermi arc touching point. The dashes indicate the Fermi arc.

vortex in $\vec{\Delta}$, as the two terms in Eq. (7) have similar magnitudes and opposite vorticities and cancel. Near the Weyl cone, however, the $\nabla_{k_\perp}\alpha$ term is negligible and only $\nabla_{k_\perp}\phi$ contributes.

The streamline plots in Fig. 2 also show that $\vec{\Delta}$ winds around a point $\vec{K}_{\rm opp}$ *opposite* to the Fermi arc touching point. However, around this point the magnitude of the beam shift scales as $|\vec{\Delta}| \sim |\vec{K} - \vec{K}_{\rm opp}|^{1/2}$. The vanishing of $\vec{\Delta}$ at $\vec{K}_{\rm opp}$ means that deviations from ideal beam trajectories, due to the internal spinor degrees of freedom, become negligible in this region of momentum space.

Paired Weyl cones.—To show that the above results are not model specific, we consider an alternative model described by the quadratic Hamiltonian [46,47]

$$H = v\begin{bmatrix} -k_y & \beta(k_x^2 - m) - ik_z \\ \beta(k_x^2 - m) + ik_z & k_y \end{bmatrix}. \quad (9)$$

This has dispersion $E = \pm v\sqrt{\beta^2(k_x^2 - m)^2 + k_y^2 + k_z^2}$, and exhibits either paired Weyl points or a complete band gap, depending on the choice of m. In the region $z > 0$, we set $m = m_0 > 0$, so that there are Weyl points at $\vec{k} = [\pm\sqrt{m_0}, 0, 0]$; there are two Weyl cones for small $|E|$, which merge into a single band for larger $|E|$. For $z < 0$, we let $m = -m_1 < 0$ to ensure a complete gap for $|E| < v\beta|m_1|$, and set E within this gap.

The calculation of the beam shift proceeds along similar lines. The form of the planar eigenmodes in the $z > 0$ region is similar to Eq. (1), and evanescent for $z < 0$. Instead of using the boundary Eq. (3), we require the components of $\psi_{\rm tot}$ to be continuous at $z = 0$. The Fermi arc is then found to be the line segment $|k_x| < \sqrt{m_0}$, $k_y = E/v$. Finally, we construct beams similar to Eq. (6) and calculate the reflected beam displacement $\vec{\Delta}$.

The resulting plots of $\vec{\Delta}$ versus $\vec{K}_\perp$ are shown in Fig. 3. The behavior is highly similar to the single-cone case, despite key differences in the calculation—not only in the Hamiltonian, but also the boundary condition implementation. There are now two Weyl cones; the cone boundaries are no longer circular, but nonetheless each cone has its own Fermi arc touching point, and $\vec{\Delta}$ exhibits a half-vortex structure around each touching point. The winding direction is opposite in the two Weyl cones, consistent with their opposite chiralities, and a numerical fit shows that the $|\vec{\Delta}| \sim |\vec{K}_\perp - \vec{K}_{\rm fa}|^{-1/2}$ scaling holds near the touching points. The behavior persists even at large values of E where the cones merge into a single band. These results indicate that these features of the beam shift are generic to Weyl media, and are not qualitatively altered by model-specific band structure features.

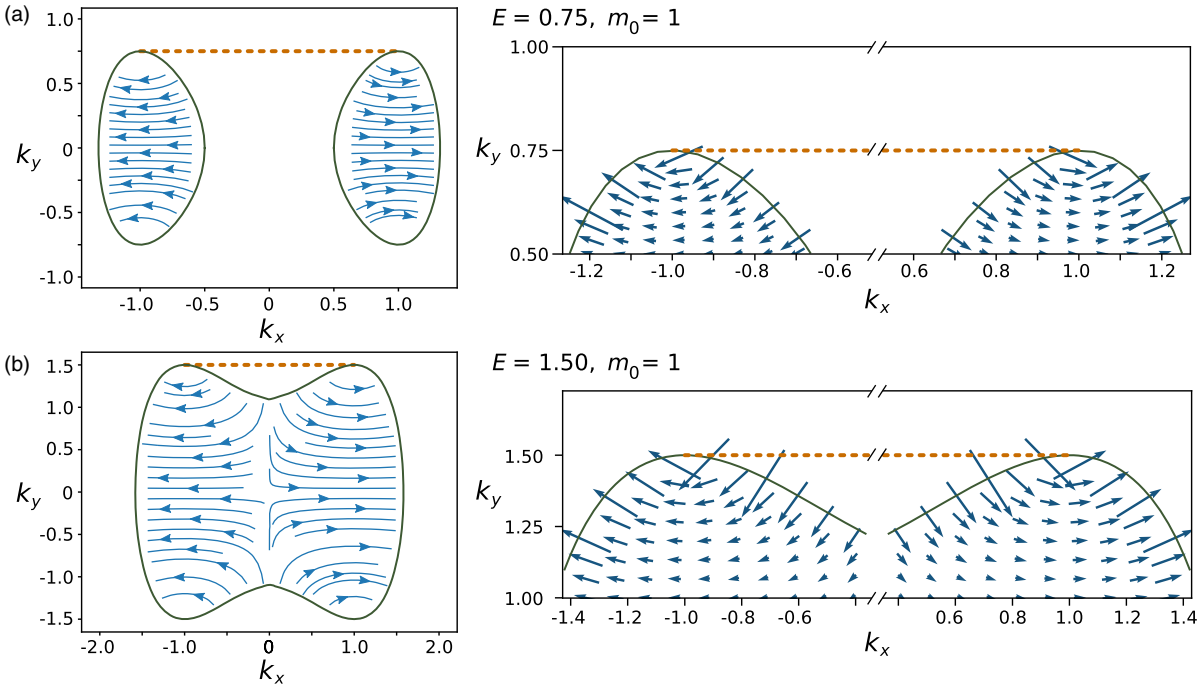

FIG. 3. Maps of the beam shift $\vec{\Delta}$, for the quadratic Hamiltonian (9) with $v = 1$, $m_0 = 1$, and $m_1 = 100$. The horizontal and vertical axes are the mean in-plane wave numbers K_x and K_y (normalized to E/v) for the incident beam. Results are shown for (a) $E = 0.75$, where the Hamiltonian describes a pair of Weyl cones, and (b) $E = 1.5$, where the two Weyl cones have merged into a single band. The left panels show a streamline plot of $\vec{\Delta}$, while the right panels show a quiver plot of $\vec{\Delta}$ near the Fermi arc touching points. The dashes indicate the Fermi arc.

Discussion.—The easiest way to observe the predicted beam shift may be to use a classical Weyl medium, such as a microwave-scale photonic crystal of the sort implemented by Lu *et al.* [26]. In a microwave experiment, a phase array can be used to generate the incident beam, and a metal surface can serve as a reflector [48]. In Ref. [26], the lattice constant is 13.4 mm and the Weyl points occur at frequency $f \approx 11.3$ GHz, with $v \approx 7 \times 10^7$ ms^{-1}. Operating 5% above the Weyl point frequency ($\delta f \approx 0.57$ GHz), the Weyl cone section has radius $K_W \approx 50$ m^{-1}. For a beam of momentum-space width $\sigma_k \approx 5$ m^{-1} (real-space width ≈100 mm), with incident beam direction such that $|\vec{K}_\perp - \vec{K}_{\rm fa}| \approx 15$ m^{-1}, the envelope has negligible overlap with the boundary of the Weyl cone. The model of Eqs. (1)–(7) then predicts $|\vec{\Delta}| \sim 46$ mm, which should be easily observable.

In solid state systems, these GH- and IF-like shifts may provide a probe for topological Fermi arc effects in Weyl semimetals and related materials. In a Weyl semimetal thin film bounded above and below by insulating media, a beam or traveling wave packet undergoes repeated reflections off the two parallel surfaces, and a straightforward calculation shows that the shifts accumulate rather than canceling out [42], producing an anomalous boost to the in-plane motion. GH shifts have been predicted to contribute to two-terminal conductance in graphene *p-n* interfaces [12], and likewise Fermi arc-induced shifts may be detectable via transport properties in thin films of Weyl semimetals. Electrons in topological semimetals have been shown to have very high mobilities [23,49], allowing multiple reflections to fit within a transport mean free path. Finally, although repeated reflections might change the beam profile, owing to higher-order terms neglected in the above calculations, one can show that the beam shift formula (7) remains valid even if the beam profile is distorted, as long as it remains a real function with a single peak in real space [42].

This work was supported by the Singapore MOE Academic Research Fund Tier 2 Grant No. MOE2015-T2-2-008, and the Singapore MOE Academic Research Fund Tier 3 Grant No. MOE2016-T3-1-006. J. C. W. S acknowledges the support of the Singapore National Research Foundation (NRF) under NRF fellowship Grant No. NRF-NRFF2016-05.

[1] R. Karplus and J. M. Luttinger, Phys. Rev. **95**, 1154 (1954).
[2] M. C. Chang and Q. Niu, Phys. Rev. Lett. **75**, 1348 (1995).
[3] M.-C. Chang and Q. Niu, Phys. Rev. B **53**, 7010 (1996).
[4] M. Onoda, S. Murakami, and N. Nagaosa, Phys. Rev. Lett. **93**, 083901 (2004).
[5] Y. D. Chong, Phys. Rev. B **81**, 052303 (2010).
[6] D. Xiao, M.-C. Chang, and Q. Niu, Rev. Mod. Phys. **82**, 1959 (2010).
[7] K. Y. Bliokh and A. Aiello, J. Opt. **15**, 014001 (2013).
[8] M. McGuirk and C. K. Carniglia, J. Opt. Soc. Am. **67**, 103 (1977).
[9] C. Imbert, Phys. Rev. D **5**, 787 (1972).
[10] M. A. Player, J. Phys. A **20**, 3667 (1987).
[11] V. G. Fedoseyev, J. Phys. A **21**, 2045 (1988).
[12] C. W. J. Beenakker, R. A. Sepkhanov, A. R. Akhmerov, and J. Tworzydło, Phys. Rev. Lett. **102**, 146804 (2009).
[13] X. Chen, X.-J. Lu, Y. Ban, and C.-F. Li, J. Opt. **15**, 033001 (2013).
[14] Y. Hatsugai, Phys. Rev. Lett. **71**, 3697 (1993).
[15] X. Wan, A. M. Turner, A. Vishwanath, and S. Y. Savrasov, Phys. Rev. B **83**, 205101 (2011).
[16] A. A. Zyuzin and A. A. Burkov, Phys. Rev. B **86**, 115133 (2012).
[17] D. T. Son and B. Z. Spivak, Phys. Rev. B **88**, 104412 (2013).
[18] A. A. Burkov, Phys. Rev. Lett. **113**, 187202 (2014).
[19] S. A. Parameswaran, T. Grover, D. A. Abanin, D. A. Pesin, and A. Vishwanath, Phys. Rev. X **4**, 031035 (2014).
[20] S. A. Yang, H. Pan, and F. Zhang, Phys. Rev. Lett. **115**, 156603 (2015).
[21] Q.-D. Jiang, H. Jiang, H. Liu, Q.-F. Sun, and X. C. Xie, Phys. Rev. Lett. **115**, 156602 (2015).
[22] J. Xiong, S. K. Kushwaha, T. Liang, J. W. Krizan, M. Hirschberger, W. Wang, R. J. Cava, and N. P. Ong, Science **350**, 413 (2015).
[23] X. Huang, L. Zhao, Y. Long, P. Wang, D. Chen, Z. Yang, H. Liang, M. Xue, H. Weng, Z. Fang *et al.*, Phys. Rev. X **5**, 031023 (2015).
[24] Q.-D. Jiang, H. Jiang, H. Liu, Q.-F. Sun, and X. C. Xie, Phys. Rev. B **93**, 195165 (2016).
[25] L. Wang and S.-K. Jian, Phys. Rev. B **96**, 115448 (2017).
[26] L. Lu, Z. Wang, D. Ye, L. Ran, L. Fu, J. D. Joannopoulos, and M. Soljačić, Science **349**, 622 (2015).
[27] W.-J. Chen, M. Xiao, and C. T. Chan, Nat. Commun. **7**, 13038 (2016).
[28] J. Noh, S. Huang, D. Leykam, Y. D. Chong, K. P. Chen, and M. C. Rechtsman, Nat. Phys. **13**, 611 (2017).
[29] B. Q. Lv, N. Xu, H. M. Weng, J. Z. Ma, P. Richard, X. C. Huang, L. X. Zhao, G. F. Chen, C. E. Matt, F. Bisti *et al.*, Nat. Phys. **11**, 724 (2015).
[30] S.-Y. Xu, I. Belopolski, N. Alidoust, M. Neupane, G. Bian, C. Zhang, R. Sankar, G. Chang, Z. Yuan, C.-C. Lee *et al.*, Science **349**, 613 (2015).
[31] N. Xu, H. M. Weng, B. Q. Lv, C. E. Matt, J. Park, F. Bisti, V. N. Strocov, D. Gawryluk, E. Pomjakushina, K. Conder *et al.*, Nat. Commun. **7**, 11006 (2016).
[32] N. P. Armitage, E. J. Mele, and A. Vishwanath, Rev. Mod. Phys. **90**, 015001 (2018).
[33] F. Li, X. Huang, J. Lu, J. Ma, and Z. Liu, Nat. Phys. **14**, 30 (2017).
[34] M. Xiao, W.-J. Chen, W.-Y. He, and C. T. Chan, Nat. Phys. **11**, 920 (2015).
[35] H. Ge, X. Ni, Y. Tian, S. K. Gupta, M.-H. Lu, X. Lin, W.-D. Huang, C. T. Chan, and Y.-F. Chen, Phys. Rev. Applied **10**, 014017 (2018).
[36] H. Wang, L. Zhou, and Y. D. Chong, Phys. Rev. B **93**, 144114 (2016).
[37] D. Z. Rocklin, B. G. Chen, M. Falk, V. Vitelli, and T. C. Lubensky, Phys. Rev. Lett. **116**, 135503 (2016).

[38] C. H. Lee, S. Imhof, C. Berger, F. Bayer, J. Brehm, L. W. Molenkamp, T. Kiessling, and R. Thomale, Commun. Phys. **1**, 39 (2018).
[39] E. McCann and V. I. Falko, J. Phys. **16**, 2371 (2004).
[40] A. R. Akhmerov and C. W. J. Beenakker, Phys. Rev. B **77**, 085423 (2008).
[41] K. Hashimoto, T. Kimura, and X. Wu, Prog. Theor. Exp. Phys. **2017**, 053I01 (2017).
[42] See Supplemental Material at http://link.aps.org/supplemental/10.1103/PhysRevLett.122.066602 for detailed derivations.
[43] H. Wang, L. Zhou, and Y. D. Chong, Phys. Rev. B **93**, 144114 (2016).
[44] W. Gao, B. Yang, M. Lawrence, F. Fang, B. Béri, and S. Zhang, Nat. Commun. **7**, 12435 (2016).
[45] Q. Wang, M. Xiao, H. Liu, S. Zhu, and C. T. Chan, Phys. Rev. X **7**, 031032 (2017).
[46] R. Okugawa and S. Murakami, Phys. Rev. B **89**, 235315 (2014).
[47] E. V. Gorbar, V. A. Miransky, I. A. Shovkovy, and P. O. Sukhachov, Phys. Rev. B **91**, 235138 (2015).
[48] D. M. Pozar, *Microwave Engineering*, 4th ed. (Wiley, New York, 2011).
[49] C. Shekhar, A. K. Nayak, Y. Sun, M. Schmidt, M. Nicklas, I. Leermakers, U. Zeitler, Y. Skourski, J. Wosnitza, Z. Liu *et al.*, Nat. Phys. **11**, 645 (2015).